



Exploration of the Molecular Mechanisms Underlying the Anti-Photoaging Effect of *Limosilactobacillus fermentum* XJC60

Huizhen Chen^{12†}, Ying Li^{2†}, Xinqiang Xie^{2†}, Moutong Chen², Liang Xue², Juan Wang², Qinghua Ye², Shi Wu², Runshi Yang², Hui Zhao², Jumei Zhang², Yu Ding^{2,3*} and Qingping Wu^{2*}

OPEN ACCESS

Edited by:

Sarah Lebeer,
University of Antwerp, Belgium

Reviewed by:

Zhi Liu,
Huazhong University of Science and
Technology, China
Zhong-Ji Qian,
Guangdong Ocean University, China

*Correspondence:

Qingping Wu
wuqp203@163.com
Yu Ding
dingyu@jnu.edu.cn

[†]These authors have contributed
equally to this work and share
first authorship

Specialty section:

This article was submitted to
Microbiome in Health and Disease,
a section of the journal
Frontiers in Cellular and
Infection Microbiology

Received: 17 December 2021

Accepted: 17 March 2022

Published: 29 April 2022

Citation:

Chen H, Li Y, Xie X, Chen M,
Xue L, Wang J, Ye Q, Wu S,
Yang R, Zhao H, Zhang J, Ding Y
and Wu Q (2022) Exploration
of the Molecular Mechanisms
Underlying the Anti-Photoaging Effect
of *Limosilactobacillus fermentum* XJC60.
Front. Cell. Infect. Microbiol. 12:838060.
doi: 10.3389/fcimb.2022.838060

¹ School of Biology and Biological Engineering, South China University of Technology, Guangzhou, China, ² Guangdong Provincial Key Laboratory of Microbial Safety and Health, State Key Laboratory of Applied Microbiology Southern China, Key Laboratory of Agricultural Microbiomics and Precision Application, Ministry of Agriculture and Rural Affairs, Institute of Microbiology, Guangdong Academy of Sciences, Guangzhou, China, ³ Department of Food Science and Technology, Institute of Food Safety and Nutrition, Jinan University, Guangzhou, China

Although lactic acid bacteria (LAB) were shown to be effective for preventing photoaging, the underlying molecular mechanisms have not been fully elucidated. Accordingly, we examined the anti-photoaging potential of 206 LAB isolates and discovered 32 strains with protective activities against UV-induced injury. All of these 32 LABs exhibited high levels of 2,2-diphenyl-picrylhydrazyl, as well as hydroxyl free radical scavenging ability (46.89–85.13% and 44.29–95.97%, respectively). Genome mining and metabonomic verification of the most effective strain, *Limosilactobacillus fermentum* XJC60, revealed that the anti-photoaging metabolite of LAB was nicotinamide (NAM; 18.50 mg/L in the cell-free serum of XJC60). Further analysis revealed that LAB-derived NAM could reduce reactive oxygen species levels by 70%, stabilize the mitochondrial membrane potential, and increase the NAD⁺/NADH ratio in UV-injured skin cells. Furthermore, LAB-derived NAM downregulated the transcript levels of matrix metalloproteinase (*MMP*)-1, *MMP*-3, interleukin (*IL*)-1 β , *IL*-6, and *IL*-8 in skin cells. *In vivo*, XJC60 relieved inflammation and protected skin collagen fiber integrity in UV-injured Guinea pigs. Overall, our findings elucidate that LAB-derived NAM might protect skin from photoaging by stabilizing mitochondrial function, establishing a theoretical foundation for the use of probiotics in the maintenance of skin health.

Keywords: *Limosilactobacillus fermentum*, skin, anti-photoaging, nicotinamide, pan-genome analysis, UV

1 INTRODUCTION

Skin aging accompanies aging in humans, manifesting as roughness, sagging, fine lines, insufficient sweating, and increased sensitivity of the skin to changes in temperature (Giangreco et al., 2008). Both internal and external factors promote skin aging, and exposure to ultraviolet (UV) rays is one of the most common and preventable external factors affecting skin aging (Kammeyer and Luiten, 2015). Skin aging caused by UV exposure, also called photoaging, contributes to more than 80% of

facial aging (Friedman, 2005; Han et al., 2014; Cavinato and Jansen-Dürr, 2017). Photoaging not only causes the deterioration of appearance but also leads to skin barrier dysfunction and even cancer (Vicentini et al., 2011). Therefore, appropriate methods for preventing photoaging are urgently needed.

After exposure to UV radiation, the amorphous elastic fibers in the skin tissue exhibit excessive accumulation, whereas the collagen fibers appear to be abnormally broken and structurally disordered, gradually forming wrinkles in the skin (Varani et al., 2004; Watson et al., 2014). Moreover, when skin cells are exposed to excessive UV radiation, reactive oxygen species (ROS) can accumulate in the cells, leading to damage to skin cells and the extracellular matrix surrounding the cells (Morita, 2007; Giangreco et al., 2008). The pathophysiological mechanisms of photoaging are mainly related to ROS-induced damage, including activation of the mitogen-activated protein kinase signaling pathway and the phosphatidylinositol 3-kinase and nuclear factor- κ B pathways and reductions in matrix metalloproteinase (MMP) synthesis and collagen production, ultimately promoting skin aging (Kammeyer and Luiten, 2015).

Skin health is not only related to skin cells but also profoundly influenced by the skin microbiome (Findley and Grice, 2014; Ladizinski et al., 2014), which is composed of millions of bacteria, fungi, and viruses. Similar to gut microbes, skin microbes play important roles in the defense against invasive pathogens, induction of immune responses, and decomposition of waste products (Scharschmidt and Fischbach, 2013; Grice, 2015; Ladizinski et al., 2014). Thus, microbiome treatment might be a novel solution for prevention of skin photoaging (Patra et al., 2020). Certain bacterial strains have major effects on improving skin conditions and preventing photoaging. For example, *Lactobacillus plantarum* HY7714 reduces skin collagen loss by affecting the activator protein-1 signaling pathway in skin cells (Kim et al., 2014; Lee et al., 2015). Further studies have suggested that the antiphotaging mechanisms of *Lacticaseibacillus rhamnosus* GG (ATCC 53103, LGG) and *Lacticaseibacillus casei* strain Shirota might be related to their antioxidant properties (Yau et al., 2020; Mai et al., 2021). Taken together, these studies have demonstrated the great potential of microbiome treatment for the alleviation of photoaging in the skin. However, the exact metabolites of probiotic strains and the molecular mechanisms through which skin microbes affect photoaging have not been fully elucidated, and the applications of microbiome treatments remain limited. Herein, we explored the molecular mechanisms through which lactic acid bacteria (LAB) exert antiphotaging effects to provide a theoretical basis for the application of probiotics in skin health care.

2 MATERIALS AND METHODS

2.1 Screening of LABs With Anti-Photoaging Activity Against UVB

2.1.1 Bacterial Isolation and Phylogenetic Analysis

We isolated 186 LAB strains from fermented foods and animal feces collected in the Xinjiang Uygur Autonomous Region and

16 LAB strains from the feces of healthy centenarians in Guangdong, China using the methods described by Zeng (Zeng et al., 2020). In addition, four standard strains (ATCC53103, ATCC7469, ATCC393, ATCC14917) were investigated as controls. Studies have demonstrated the antioxidant properties of these four strains, and they were applied to improve various diseases (Lin et al., 2009; Zahran et al., 2017; Mantzourani et al., 2018; Xu et al., 2018; Liu et al., 2021).

Genomic DNA from all LAB was extracted using a genomic DNA extraction kit (Magen Biotech, Guangzhou, Guangdong, China). LAB species were identified by an evaluation of 16S rRNA gene sequences. The 16S rRNA gene was amplified using universal primers (27F, 5'-AGAGTTTGTACCTGGCTCAG-3'; 1492R, 5'-ACGGCTACCTTGTACGACTT-3'), as described by Garrity (Garrity, 2016). The polymerase chain reaction products were sent to GENEWIZ (Suzhou, China) for Sanger sequencing, and the results were compared with reference sequences from GenBank (<http://www.ncbi.nlm.nih.gov/BLAST>) to confirm the LAB taxonomy.

2.1.2 Cell Culture

HaCaT primary human keratinocytes were obtained from Dr. Chen (First Affiliated Hospital of Sun Yat-sen University) and maintained at 37°C in a 5% CO₂ incubator (ThermoFisher Scientific, Waltham, MA, USA) in complete medium containing Dulbecco's modified Eagle's medium (ThermoFisher Scientific) with 10% (v/v) fetal bovine serum (Gibco, NY, USA) and antibiotics-antimycotic (100 U penicillin, 100 µg/mL streptomycin, and 0.25 µg/mL amphotericin B; HyClone, UT, USA).

2.1.3 Minimum Nontoxic Dilution (MNTD) Preparation

All LAB were grown in de Man Rogosa Sharpe (MRS) broth (HuanKai Microbial, Guangzhou, Guangdong, China) at 37°C for 48 h in an anaerobic workstation (Don Whitley Scientific, W Yorkshire, UK). The cells were pelleted by centrifugation at 10,000 × g at 4°C for 10 min, and supernatants were collected using 0.22 µm microfilters (HuanKai Microbial). Cell-free supernatants (CFSs) and uninoculated MRS broth controls were adjusted to pH 7.35–7.45 using sodium hydroxide (Sigma-Aldrich, St. Louis, MO, USA) and stored at –80°C until use. The cytotoxicity of the pH-adjusted CFS samples was assessed using Cell Counting Kit-8 (CCK-8) assays (GLPBIO, Montclair, CA, USA) according to the manufacturer's instructions. Five-fold dilutions of CFSs were generated, and the cytotoxicity of each CFS was re-evaluated if HaCaT cell viability failed to remain at 100% after 24 h of incubation with 10% CFSs in complete cell medium. The CFSs with the lowest toxicity were defined as the MNTDs.

2.1.4 UVB Exposure in HaCaT Cells

HaCaT cells were seeded in 96-well plates at a density of 1×10^5 cells/well and grown for 24 h to reach 80% confluency. After replacing cell supernatants with 100 µL phosphate-buffered saline, HaCaT cells were exposed to UVB at 18 mJ/cm² for 5 min using a UVB-313EL light tube (ANTOINE, Guangzhou,

Guangdong, China). The supernatants were changed to 100 μ L complete cell medium after UV radiation for subsequent studies.

2.1.5 High-Throughput Assay to Screen for the Anti-UVB Potential of MNTDs

The viability of HaCaT cells treated with MNTDs of LAB at 24 h after UVB exposure was examined to screen for the antiphotaging potential of LAB. Briefly, the viability of UVB-exposed cells was tested after incubation for 24 h with 10% MNTDs in complete cell medium using a CCK-8 kit (GLPBIO). pH-adjusted MRS-treated cell suspensions were used as a positive control, and complete cell medium was used as a negative control. Absorbance at 450 nm was then quantified with a microplate reader (Biotek, Winooski, VT, USA).

2.2 Evaluation of Antioxidant Effects of LABs

2.2.1 Free Radical Scavenging Ability

Because antioxidant ability can be the main reason for the antiphotaging effects of LAB (Han et al., 2014), we evaluated the 2,2-diphenyl-picrylhydrazyl (DPPH) and hydroxyl radical-scavenging activities of the MNTDs for 206 LAB strains. The method of Shimada was used to assess the DPPH free radical-scavenging ability of the MNTDs of different LAB. Briefly, 100 μ L MNTDs was added to 100 μ L of 0.2 mM methanolic solution of DPPH (Yuanye Biology, Shanghai, China) and incubated in the dark at room temperature for 30 min. The absorbance of the resulting solution was measured at 517 nm with a microplate reader (Biotek). Distilled water was used as a control in the test. The DPPH free radical-scavenging activity was calculated using the following formula.

DPPH radical scavenging capability (%)

$$= \frac{A_C - A_S}{A_C} \times 100 \quad (1)$$

In this formula, A_S is the absorbance value of MNTDs, and A_C is the absorbance value of the control.

The scavenging ability of hydroxyl radicals was determined using the method described by Liu (Liu et al., 2009). A mixture of 30 μ L of 0.75 mM 1,10-phenanthroline (MACKLIN, Shanghai, China), 30 μ L of 0.75 mM FeSO_4 (Chemical Reagent, Guangzhou, Guangdong, China), 30 μ L of 0.01% (v/v) H_2O_2 , 60 μ L of 0.2 M (pH 7.4) sodium phosphate buffer, and 30 μ L MNTDs was incubated at 37°C for 60 min, and the absorbance of the mixture was measured at 536 nm with a microplate reader (Biotek).

Hydroxyl radical scavenging activity (%)

$$= \frac{A_S - A_C}{A_0 - A_C} \times 100 \quad (2)$$

In this formula, A_0 is the absorbance of deionized water instead of H_2O_2 , A_S is the absorbance value of CFS, and A_C is the absorbance without CFS.

2.2.2 ROS Generation Assay

Intracellular ROS levels were measured using a Reactive Oxygen Species Assay Kit (Beyotime Biotechnology, Shanghai, China). Briefly, the cells were seeded in 6-well plates and exposed to UV radiation as described. The cells were then treated with 10% MNTDs from different LAB. Following treatment, the cells were incubated with DCFH-DA for 20 min at 37°C in the dark, and fluorescence was measured using a BD FACSCanto II Flow Cytometer (BD Biosciences, San Jose, CA, USA). pH-adjusted MRS-treated cell suspensions were chosen as the negative control. Fluorescence images were acquired using a CYTATION 5 Imager Reader (Biotek).

2.3 Genomic Mining of the Anti-Photoaging Metabolites of LABs

2.3.1 Genomic DNA Library Preparation

Genomic DNA libraries were constructed using AMT Rapid DNA-Seq Kits for Illumina (CISTRO, Guangzhou, Guangdong, China), with fragmentation, end-repair, adaptor ligation with Illumina adapters, size selection with beads, and library DNA amplification; all methods were performed according to the manufacturer's instructions. The libraries were assessed using an Agilent Bioanalyzer 2100 (Agilent Technologies, Santa Clara, CA, USA) and a Qubit 3.0 fluorometer (Invitrogen, Carlsbad, CA, USA). DNA sequencing was performed on an Illumina Nextseq 550 platform (Illumina, San Diego, CA, USA) with a High Output v2.5 kit (Illumina). Long reads of microbial genomic DNA libraries were prepared using a Rapid Barcoding Sequencing Kit (Nanopore, Oxford, UK) and sequenced on a Nanopore MinION platform with R9.4.1 flow cells (Nanopore).

Low-quality reads from Illumina sequencing were filtered out using Trimmomatic software (v0.39) (Bolger et al., 2014). Low-quality and short reads from Nanopore sequencing were filtered using Filtlong software (v0.2.0; <https://github.com/rrwick/Filtlong>). The filtered Illumina and Nanopore reads were aligned into *de novo* assembled contigs using Unicycler software (v0.4.8) (Nurk et al., 2013).

2.3.2 Genome Annotations and Comparative Genomics Analysis

Pan-genome analysis was performed on the Prokka output using Roary (v3.11.2) with a BLASTP identity cut-off of 95% (Page et al., 2015). The LAB strain core-genome was produced using Harvest software (v1.1.2), with ATCC 14931 as the reference genome (Treangen et al., 2014). Following core-genome alignment, Gubbins was used for recombination analysis and the removal of putative recombined regions (Croucher et al., 2015).

2.3.3 Nicotinamide Quantitation

A Shimadzu high-performance liquid chromatography (HPLC) system (Shimadzu, Tokyo, Japan), equipped with an LC-20A UV detector (Shimadzu), was used with a COCOSMOSIL 5C18-PAQ column (5 μ m, 4.6 mm \times 250 mm) for the separation of compounds. The temperature of the column compartment was maintained at 30°C throughout the analysis. The wavelength of

detection was 254 nm, and the injection volume was 20 μ L. All chromatographic assays were performed with a flow rate of 1 mL/min, and 25 mM potassium dihydrogen phosphate buffer was used as the mobile phase. The method was validated by checking the accuracy, precision, linearity, limit of detection, limit of quantitation, and specificity prior to sample analysis.

2.4 Study of the Anti-Photoaging Mechanism of *L. fermentum* XJC60 and Nicotinamide

2.4.1 Measurement of Mitochondrial Membrane Potential

Intracellular mitochondria membrane potential levels were measured using a Mitochondria Membrane Potential Kit (Sigma-Aldrich). Briefly, the cells were collected from the plates and incubated with 500 μ L JC-10 Dye Loading Solution for 15 min at 37°C in the dark. Fluorescence was measured using a BD FACSCanto II Flow Cytometer (BD Biosciences). pH-adjusted MRS-treated cell suspensions were used as the negative control.

2.4.2 Analysis of NAD⁺/NADH Levels

After treatment of HaCaT cells (1×10^6 cells/sample), cells were collected, and intracellular NAD⁺ levels were determined using an NAD⁺/NADH assay kit with WST-8 (Beyotime Biotechnology). Briefly, cells were lysed with 200 μ L cold lysis buffer. To measure total NAD⁺ and NADH concentrations, 20 μ L of cell lysate was added to each well of a 96-well plate. To measure NADH levels, lysed cell suspensions were incubated at 60°C for 30 min, and 20 μ L was then added to each well of a 96-well plate. Subsequently, 90 μ L alcohol dehydrogenase was added to each well, and the plates were incubated at 37°C for 10 min. Finally, 10 μ L chromogenic solution was added, and the mixture was incubated at 37°C for 30 min. A standard curve was generated and measured at the same time as the samples. The absorbance values were measured at 450 nm and analyzed on a microplate reader (Biotek). The amount of NAD⁺ was derived by subtracting NADH from total NAD⁺/NADH. pH-adjusted MRS-treated cell suspensions were used as the negative control.

2.5 Evaluation of the Anti-Photoaging Effect of *L. fermentum* XJC60 and Nicotinamide *In Vitro*

2.5.1 Enzyme-Linked Immunosorbent Assay (ELISA)

After treating HaCaT cells (1×10^6 cells/sample), cells were collected, and MMP-1 concentrations were determined using an MMP-1 ELISA kit (Bosterbio, Pleasanton, CA, USA) according to the manufacturer's protocol. pH-adjusted MRS-treated cell suspensions were used as the negative control.

2.5.2 Reverse Transcription Polymerase Chain Reaction (RT-PCR)

After treating HaCaT cells (1×10^6 cells/sample), cells were collected, and RNA was extracted using a HiPure Total RNA Mini Kit (Magen). cDNA was synthesized from 1 μ g of total RNA using Evo M-MLV reverse transcriptase (Accurate Biology

AG, Changsha, Hunan, China) according to the manufacturer's instructions. Primers for *MMP-1*, *MMP-3*, interleukin (IL)-1 β , *IL-6*, *IL-8*, and glyceraldehyde 3-phosphate dehydrogenase (*GAPDH*), which were used for semiquantitative RT-PCR (Supplementary Table S1), were synthesized by GENEWIZ. The qPCR assay was performed using a LightCycler96 (Roche Diagnostics Corporation, Indianapolis, IN, USA) using the following conditions: 95°C for 30 s; 40 cycles of 95°C for 5 s, 60°C for 30 s, 95°C for 5 s, 60°C for 60 s, and 95°C for 1 s. Data were analyzed using LightCycler96 SW software (Roche Diagnostics Corporation).

2.6 Evaluation of the Anti-Photoaging Effect of *L. fermentum* XJC60 *In Vivo*

2.6.1 Experimental Animals and Topical Administration

Six female Dunkin Hartley Guinea pigs (weight: 250–350 g) were purchased from the Laboratory Animal Center of Southern Medical University (Guangzhou, Guangdong, China) and were allowed to acclimate for 1 week before the experiment. The animals were housed in a climate-controlled facility with a temperature of 24°C, humidity of 50%, dark/light cycle of 12:12 h, and free access to food and water. All experimental protocols were approved by the Institutional Animal Care and Use Ethics Committee of Institute of Microbiology, Guangdong Academy of Science (approval no. GT-IACUC202010225).

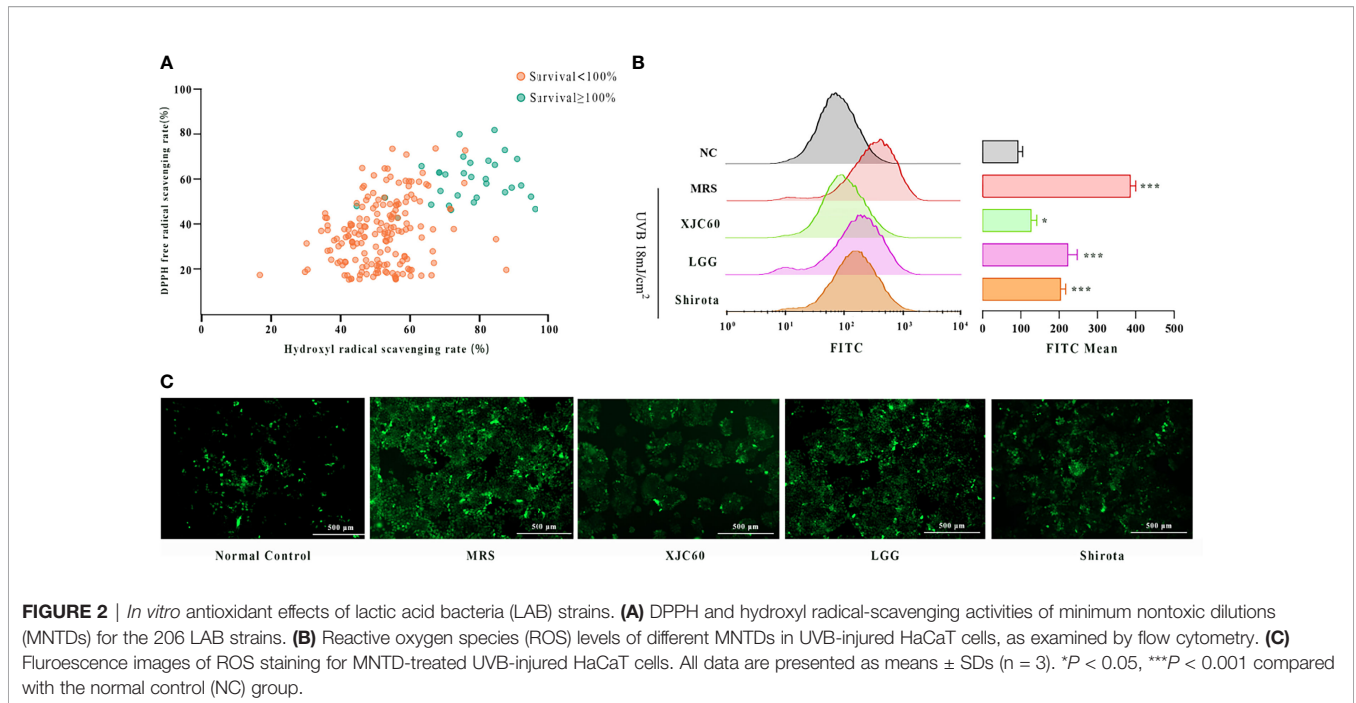
The methods used for the animal experiment were obtained from the Cosmetic Safety Technical Specification. Briefly, 18–24 h prior to the UVB damage test, the back skin of each animal was depilated. The skin at the test site was intact and free of damage. The depilated skin was divided into four zones, each measuring approximately 2 cm \times 2 cm. The four zones were treated as follows: zone 1 was the test group (0.2 mL MNTDs from *Limosilactobacillus fermentum* XJC60 [$n = 6$] was applied externally after UVB irradiation [75 mJ/cm²]); zone 2 was the control group (0.2 mL pH-adjusted MRS [$n = 6$] was applied externally after UVB irradiation [75 mJ/cm²]); and zones 3 and 4 were the blank control group without UVB radiation but treated with 0.2 mL *L. fermentum* XJC60 or pH-adjusted MRS externally.

2.6.2 Histological Analyses

Histological analyses were performed on hematoxylin/eosin (H&E)-stained skin samples fixed in 4% paraformaldehyde, embedded in paraffin, and stained using an H&E Stain Kit (Solarbio Life Science, Beijing, China). Images were captured using a flat-panel microscope for analysis (Kangtao Technology, Wuhan, Hubei, CHINA).

2.7 Statistical Analysis

Data analysis was performed using t-tests or by one-way analysis of variance with GraphPad Prism Software (GraphPad, La Jolla, CA, USA). Results with *P* values of less than 0.05 were considered statistically significant. Data are presented as means \pm standard deviations (SDs) of at least three independent experimental replicates.



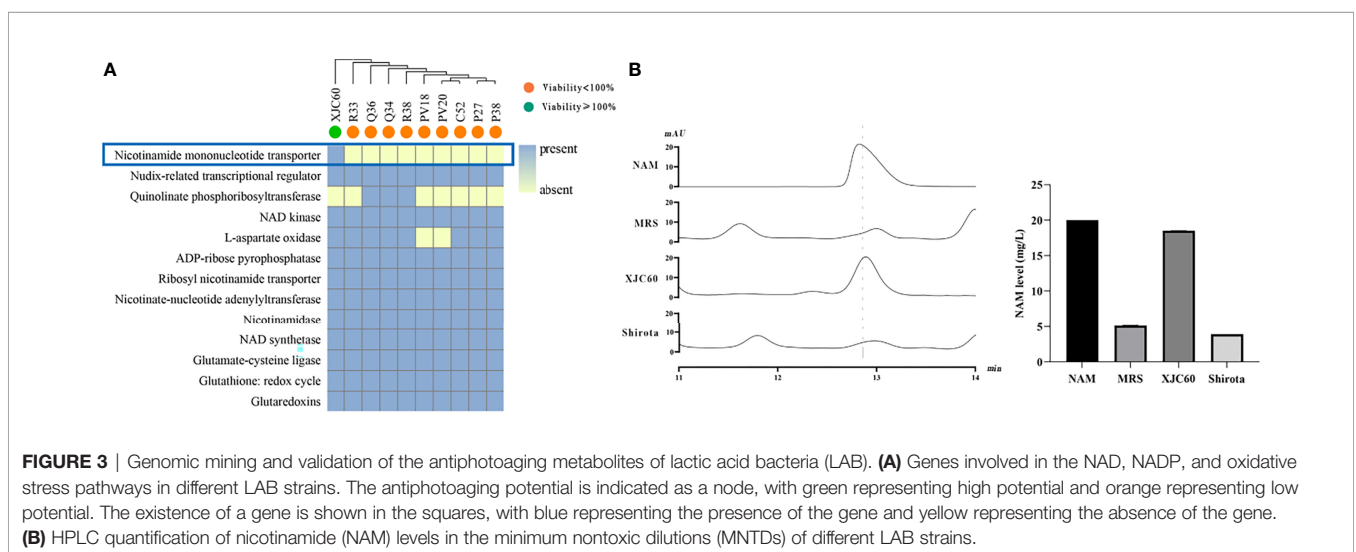
8.74 versus 288.70 ± 12.50 for the JC-1 level, *P* = 0.131; **Figure 4**). Taken together, these results indicated that LAB-derived NAM is an essential metabolite mediating antiphotaging activity in UVB-injured HaCaT cells.

3.5 *In Vitro* Assessment of the Antiphotaging Potential of LAB-Derived NAM

Wrinkles and roughness of photoaged skin are mainly related to degradation and inflammation of skin cells (Makrantonaki et al., 2013). Therefore, we further analyzed the antiphotaging effects of LAB-derived NAM. ELISA showed that LAB-derived NAM effectively reduced the amount of MMP-1 from 4323.00 ± 366.90 pg/mL to 3712.00 ± 63.06 pg/mL (*P* = 0.020), and similar

changes were observed for NAM-containing MRS (3786.00 ± 290.30 pg/mL, *P* = 0.010; **Figure 5A**).

We also evaluated the antiphotaging potential of LAB-derived NAM at the transcript level in HaCaT cells. Our results showed MMP-1 mRNA levels were significantly downregulated by 14.02-fold by the MNTD of *L. fermentum* XJC60 (*P* = 0.002). Additionally, MMP-3, IL-1 β , IL-6, and IL-8 were downregulated by 4.32-fold (*P* = 0.001), 2.29-fold (*P* < 0.001), 3.24-fold (*P* < 0.001), and 4.89-fold (*P* = 0.001), respectively. We also examined the antiphotaging effects of NAM-containing MRS and found similar changes in the mRNA levels of MMPs and inflammation-related factors (*P* > 0.05 compared to those with the MNTD of *L. fermentum* XJC60). Together, these results indicated that the NAM produced by *L.*



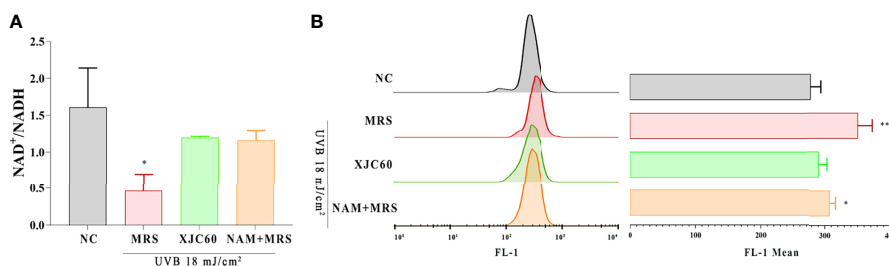


FIGURE 4 | Evaluation of mitochondrial protection by *Limosilactobacillus fermentum*-derived nicotinamide (NAM). **(A)** Effects of minimum nontoxic dilutions (MNTDs) on the NAD⁺/NADH ratio in *L. fermentum* XJC60 and equal amounts of NAM on UVB-injured HaCaT cells. **(B)** Flow cytometric analysis of JC-1 levels with different MNTDs in LAB. Data are presented as means ± SDs (n = 3). *P < 0.05, **P < 0.01 compared with the NC group.

fermentum exerted strong antiphotaging effects through the inhibition of MMPs and inflammation in UVB-injured keratinocytes (Figure 5B).

3.6 In Vivo Antiphotaging Effects of *L. fermentum* XJC60

To evaluate the antiphotaging effects of the MNTD of *L. fermentum* XJC60, pathological changes were investigated in H&E-stained skin sections. Compared with that in non-irradiated tissues, UVB radiation induced abnormal keratinization in the skin of Guinea pigs, with obvious proliferation, visible epithelial edema, and mild cell necrosis (Figure 6). Furthermore, the topical application of the MNTD of *L. fermentum* XJC60 significantly alleviated UVB damage, which was characterized by a complete skin tissue structure, orderly arrangement of the dermis and epidermis, and abundant and complete subcutaneous hair follicles and sebaceous glands (Figure 6). This also confirmed the previous results in section 3.5; specifically, the external application of the MNTD of *L. fermentum* XJC60 reduced the high MMP-1 levels in epidermal cells caused by UVB irradiation, and thus, the abnormal keratinization and hyperplasia of the Guinea pig epidermis was improved. In addition, there was no edema and inflammatory cell infiltration in the XJC60 group, which was attributed to the decreased expression of inflammatory factors in the skin of Guinea pigs induced by the MNTD of *L. fermentum* XJC60.

4 DISCUSSION

With the development of next-generation sequencing, we found that skin microbes play vital roles in skin function, thereby affecting the health of the skin and even the whole body (Scharschmidt and Fischbach, 2013). In fact, research showed the species richness of the skin microecology gradually increases with age, hinting at a correlation between the skin microbiota and aging (Ying et al., 2015; Li et al., 2020; Luna, 2020). However, the specific mechanisms through which the skin microbiome mediates skin aging remain unclear, and further studies at the cellular level are needed.

Photaging is caused by oxidative damage and decreased collagen synthesis in skin cells after exposure to UV radiation (Kammeyer and Luiten, 2015). Previous studies have demonstrated that photaging is related to certain microorganisms, and probiotics can have antiphotaging effects (Li et al., 2020). For example, *Lactobacillus acidophilus* KCCM12625 can significantly suppress ROS generation in UVB-injured skin cells, thereby reducing the photaging phenomenon caused by oxidative damage (Lim et al., 2020). However, the molecular mechanisms mediating the antiphotaging effects of probiotics have not yet been thoroughly analyzed.

Multomics-based microbial function mining provides a new approach for the exploration of molecular mechanisms. For example, Lloyd-Price used a multomics database to explore the relationships between intestinal microbial activities and inflammatory bowel disease and explained the key functions of acylcarnitines from *Clostridia* in disease progression (Lloyd-Price et al., 2019). Such studies have illustrated that the key factors through which the microbiome affects human health are active microbiologic metabolites (Koh et al., 2016). Therefore, this strategy might be a practical approach for an analysis of the functions of key microbial metabolites in human health, and we expect that there could be a similar mechanism between skin microecology and photaging.

In this study, we combined pan-genomic and metabolomic methods to explore the key metabolites of probiotics that protect against photaging and their mechanisms of action. We tested 206 LAB isolates from different sources and found that 32 isolates had protective effects on UVB-damaged skin cells, suggesting potential applications in the prevention of photaging (Figure 1). Furthermore, the results revealed that 32 strains providing protection against UVB injury had stronger antioxidant activities than those without significant protective effects from radicals (Figure 2A). The strong anti-photaging potential of *L. fermentum* XJC60 significantly reduced the high ROS level in UVB-damaged HaCaT cells (Figures 2B, C). Therefore, we found that a reduction in intracellular oxidative stress was the main antiphotaging mechanism of LAB. Indeed, LAB fermentation broth contained a variety of antioxidant factors, which could quickly degrade free radicals and hydroxyl groups, reduce intracellular ROS production, and repair photaging cells.

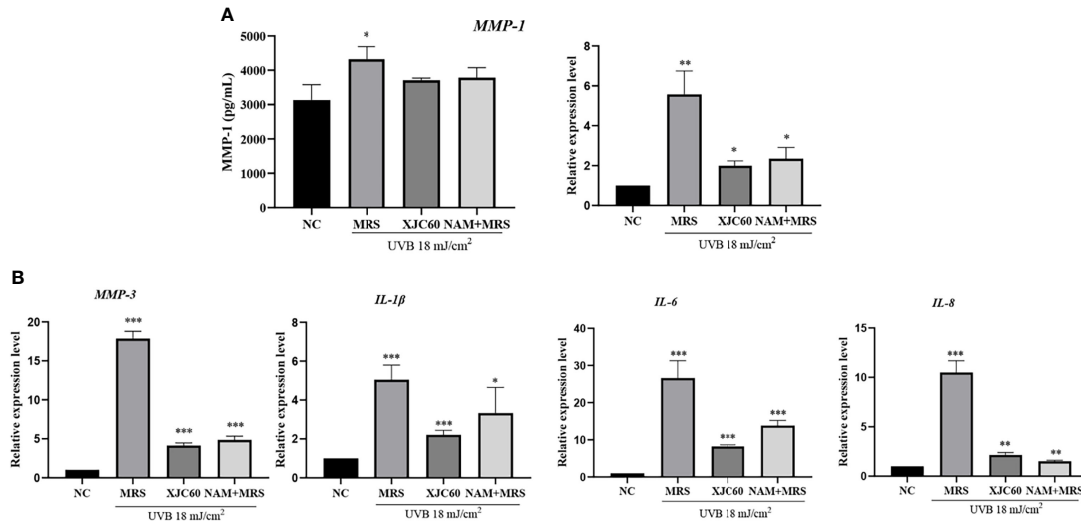


FIGURE 5 | Effects of *Limosilactobacillus fermentum* XJC60 and nicotinamide (NAM) on ECM and inflammation in UVB-injured HaCaT cells. **(A)** Evaluation of MMP-1 protein and mRNA levels. **(B)** mRNA levels of other MMPs and inflammation-related factors. Relative mRNA levels of *MMP-1*, *MMP-3*, *IL-1β*, *IL-6*, and *IL-8* in UVB-injured HaCaT cells were calculated using qPCR, with normalization to *GAPDH* expression. Data are presented as means ± SDs (n = 3). **P* < 0.05, ***P* < 0.01, ****P* < 0.001 compared with the normal control (NC) group.

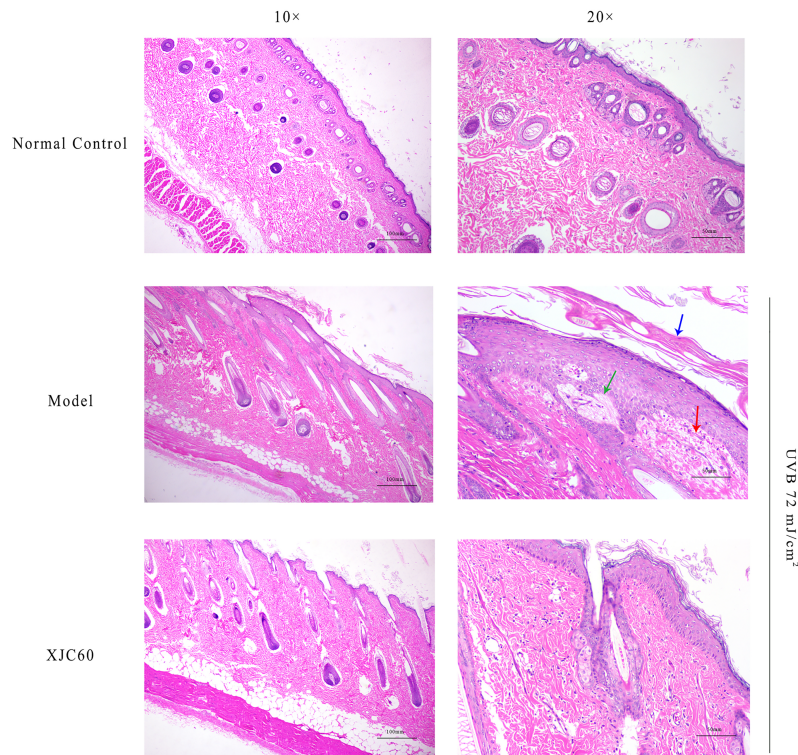


FIGURE 6 | *In vivo* antiphotaging effects of *Limosilactobacillus fermentum* XJC60. (Normal control) Left: smooth stratum corneum and obvious keratinized beads (10×); right: no inflammatory cell infiltration or cell necrosis was detected (20×). (Model) Left: abnormal keratinization in the skin of Guinea pigs, with obvious proliferation (10×); right: visible epithelial edema and mild cell necrosis (20×). Blue arrow: keratinization; green arrow: epithelial edema; red arrow: cell necrosis. (*L. fermentum* XJC60) Left: the skin tissue structure was relatively complete, keratinization of the skin was reduced, and keratinization beads were being repaired (10×); right: no inflammatory cell infiltration or cell necrosis were observed (20×).

Furthermore, we used pan-genomics combined with metabolomics to identify key metabolites mediating the antiphotaging effects of LAB. Data mining revealed a strain-specific protein, nicotinamide mononucleotide transporter, which promoted antioxidant activity in *L. fermentum* XJC60 (**Figure 3A**). Nicotinamide mononucleotide transporter can directly transport extracellular NMN into the cell and increase the level of NAM, thereby regulating NAD⁺ metabolism (Wu and Sinclair, 2019; Lloyd-Price et al., 2019; Yachida et al., 2019). We further quantified the LAB metabolites by HPLC and found high levels of NAM (18.50 mg/L) in culture broth from the MNTD of *L. fermentum* XJC60 (**Figure 3B**), validating the pan-genomics results. Previous studies have demonstrated the protective effects of NAM on photoaging, and clinical trials have demonstrated that oral nicotinamide can prevent UV-induced immunosuppression and photocarcinoma (Yiasemides et al., 2009; Park et al., 2010; Thompson et al., 2015). In particular, this is the first study demonstrating that NAM produced by LAB also exhibit strong antiphotaging effects. These results suggest that XJC60 might repair the oxidative stress state through the NAD⁺ pathway, thereby maintaining the normal homeostasis of UV-damaged skin cells and ultimately delaying skin photoaging.

As part of glycolysis and the tricarboxylic acid cycle, NAD⁺ is an important cofactor for cell respiration metabolism, and the NAD⁺/NADH level affects the normal progression of complex I in the mitochondrial respiratory chain (Fania et al., 2019). If the level of NAD⁺/NADH is too low, the mitochondrial respiratory chain will be disrupted, and the production of ATP will halt owing to impairments in calcium flow in the cell; this then reduces mitochondrial membrane potential and blocks mitochondrial function (Brand et al., 2018; Owens et al., 2013). Our findings also showed that LAB-derived NAM could significantly increase the levels of NAD⁺/NADH and recover mitochondrial membrane potential in UVB-injured HaCaT cells (**Figure 4**). Because the mitochondrial respiration program damaged by UVB was repaired, the energy-dependent DNA repair mechanism could be restored to normal (Holmström and Finkel, 2014). Therefore, produced as a by-product of the respiratory chain, the ROS level was also reduced, the oxidative stress in skin cells was alleviated, and cell viability returned to normal (**Figures 1, 2**). In addition, UV-induced ROS stimulates the synthesis of MMPs and pro-inflammatory factors, leading to the degradation of collagen and typical symptoms of inflammation and dry, peeling skin (Scharffetter-Kochanek et al., 2000). In our study, LAB-derived NAM reduced the expression levels of MMPs and ILs in UVB-injured HaCaT cells and prevented abnormal keratinization, epithelial edema, and inflammatory cell infiltration *in vivo* (**Figures 5, 6**).

However, there were still some limitations to our study. Although our results indicated that *Lactobacillus*-derived NAM is an important metabolite protecting against photoaging in *L. fermentum* XJC60, we also found that its MNTDs resulted in stronger protection for skin cells than a similar dose of NAM. This result suggested that there might be some other active

substances in *L. fermentum* XJC60 that should be explored. In addition, we only evaluated the functions of LAB-derived metabolites; the effects of live bacteria on UV-damaged skin have not yet been elucidated. Therefore, further studies are needed to assess the interactions between LAB and UV-damaged skin.

5 CONCLUSIONS

In this study, we combined pan-genomics and metabolomics to identify new antiphotaging factors from metabolites of LAB strains with antiphotaging potential. We discovered that the NAM mononucleotide transporter produced by LAB was beneficial for the synthesis of NAM, which might be a key metabolite for skin protection. Furthermore, we demonstrated that LAB-derived NAM could stabilize mitochondrial function and reduce ROS generation in UVB-injured skin cells, thereby suppressing collagen degradation and inflammation *in vitro* and *in vivo*. In addition, our results suggested that there might be some other active substances in LAB, which should be explored further. Overall, our findings provided insights into the antiphotaging mechanisms of probiotics and established novel approaches for the maintenance of skin health using LAB-derived NAM as an antiphotaging treatment.

DATA AVAILABILITY STATEMENT

The datasets presented in this study can be found in online repositories. The name of the repository and accession numbers can be found below: NCBI; PRJNA703332, PRJNA703368, PRJNA703369, PRJNA703370, PRJNA703371, PRJNA703372, PRJNA703373, PRJNA703374, PRJNA703375, PRJNA703376.

ETHICS STATEMENT

The animal study was reviewed and approved by the Institutional Animal Care and Ethics Committee of Institute of Microbiology, Guangdong Academy of sciences.

AUTHOR CONTRIBUTIONS

Conceptualization, HC, YL, XX, and QW. Methodology, HC, YL, LX, QY, and RY. Software, HC, YL, XX, LX, and SW. Validation, HC, YL, MC, LX, HZ, and MC. Formal analysis, HC, YL, MC, and YD. Investigation, HC, YL, LX, JW, and XX. Resources, XX, JW, JZ, and YD. Data curation, YL and XX. Writing—original draft preparation, HC and YL. Writing—review and editing, XX, QY, HZ, RY, YD, and QW. Visualization, HC, SW, and JW. Supervision, XX, YD, and QW. Project administration, JZ, YD, and QW. Funding acquisition, XX, YD, and QW. All authors contributed to the article and approved the submitted version.

FUNDING

This study was jointly supported by research grants from Project by the Department of Science and Technology of Guangdong Province (2019QN01N107), Key Laboratory of Guangdong Province (2020B121201009), the Guangdong Province Academy of Sciences Special Project for Capacity Building of Innovation Driven Development (2020GDASYL-20200301002). The funders had no role in the design of the study, in the collection, analyses, or interpretation of data, in

the writing of the manuscript, or in the decision to publish the results.

REFERENCES

- Birch-Machin, M. A. (2000). Mitochondria and Skin Disease. *Clin. Exp. Dermatol.* 25(2), 141–146. doi: 10.1046/j.1365-2230.2000.00605.x
- Bolger, A. M., Lohse, M., and Usadel, B. (2014). Trimmomatic: A Flexible Trimmer for Illumina Sequence Data. *Bioinformatics* 30(15), 2114–2120. doi: 10.1093/bioinformatics/btu170
- Brand, R. M., Wipf, P., Durham, A., Epperly, M. W., Greenberger, J. S., and Faló, L. D. Jr. (2018). Targeting Mitochondrial Oxidative Stress to Mitigate UV-Induced Skin Damage. *Front. Pharmacol.* 9, 920. doi: 10.3389/fphar.2018.00920
- Cavinato, M., and Jansen-Dürr, P. (2017). Molecular Mechanisms of UVB-Induced Senescence of Dermal Fibroblasts and its Relevance for Photoaging of the Human Skin. *Exp. Gerontol.* 94, 78–82. doi: 10.1016/j.exger.2017.01.009
- Croucher, N. J., Page, A. J., Connor, T. R., Delaney, A. J., Keane, J. A., Bentley, S. D., et al. (2015). Rapid Phylogenetic Analysis of Large Samples of Recombinant Bacterial Whole Genome Sequences Using Gubbins. *Nucleic Acids Res.* 43(3), e15. doi: 10.1093/nar/gku1196
- Elefantova, K., Lakatos, B., Kubickova, J., Sulova, Z., and Breier, A. (2018). Detection of the Mitochondrial Membrane Potential by the Cationic Dye JC-1 in L1210 Cells With Massive Overexpression of the Plasma Membrane ABCB1 Drug Transporter. *Int. J. Mol. Sci.* 19(7), 1985. doi: 10.3390/ijms19071985
- Fania, L., Mazzanti, C., Campione, E., Candi, E., Abeni, D., and Dellambra, E. (2019). Role of Nicotinamide in Genomic Stability and Skin Cancer Chemoprevention. *Int. J. Mol. Sci.* 20(23), 5946. doi: 10.3390/ijms20235946
- Finamore, A., Ambra, R., Nobili, F., Garaguso, I., Raguzzini, A., and Serafini, M. (2018). Redox Role of *Lactobacillus Casei* Shirota Against the Cellular Damage Induced by 2,2'-Azobis (2-Amidinopropane) Dihydrochloride-Induced Oxidative and Inflammatory Stress in Enterocytes-Like Epithelial Cells. *Front. Immunol.* 9, 1131. doi: 10.3389/fimmu.2018.01131
- Findley, K., and Grice, E. A. (2014). The Skin Microbiome: A Focus on Pathogens and Their Association With Skin Disease. *PLoS Pathog.* 10(11), e1004436. doi: 10.1371/journal.ppat.1004436
- Friedman, O. (2005). Changes Associated With the Aging Face. *Facial Plast. Surg. Clin. North Am.* 13(3), 371–380. doi: 10.1016/j.fsc.2005.04.004
- Garrity, G. M. (2016). A New Genomics-Driven Taxonomy of Bacteria and Archaea: Are We There Yet? *J. Clin. Microbiol.* 54(8), 1956–1963. doi: 10.1128/JCM.00200-16
- Giangreco, A., Qin, M., Pintar, J. E., and Watt, F. M. (2008). Epidermal Stem Cells are Retained *In Vivo* Throughout Skin Aging. *Aging Cell.* 7(2), 250–259. doi: 10.1111/j.1474-9726.2008.00372.x
- Grice, E. A. (2015). The Intersection of Microbiome and Host at the Skin Interface: Genomic- and Metagenomic-Based Insights. *Genome Res.* 25(10), 1514–1520. doi: 10.1101/gr.191320.115
- Han, A., Chien, A. L., and Kang, S. (2014). Photoaging. *Dermatol. Clin.* 32(3), 291–9, vii. doi: 10.1016/j.det.2014.03.015
- Holmström, K. M., and Finkel, T. (2014). Cellular Mechanisms and Physiological Consequences of Redox-Dependent Signalling. *Nat. Rev. Mol. Cell Biol.* 15(6), 411–421. doi: 10.1038/nrm3801
- Kammeyer, A., and Luiten, R. M. (2015). Oxidation Events and Skin Aging. *Ageing Res. Rev.* 21, 16–29. doi: 10.1016/j.arr.2015.01.001
- Kim, H. M., Lee, D. E., Park, S. D., Kim, Y. T., Kim, Y. J., Jeong, J. W., et al. (2014). Oral Administration of *Lactobacillus Plantarum* HY7714 Protects Hairless Mouse Against Ultraviolet B-Induced Photoaging. *J. Microbiol. Biotechnol.* 24(11), 1583–1591. doi: 10.4014/jmb.1406.06038
- Koh, A., De Vadder, F., Kovatcheva-Datchary, P., and Bäckhed, F. (2016). From Dietary Fiber to Host Physiology: Short-Chain Fatty Acids as Key Bacterial Metabolites. *Cell* 165(6), 1332–1345. doi: 10.1016/j.cell.2016.05.041
- Ladizinski, B., McLean, R., Lee, K. C., Elpern, D. J., and Eron, L. (2014). The Human Skin Microbiome. *Int. J. Dermatol.* 53(9), 1177–1179. doi: 10.1111/ijd.12609
- Lee, D. E., Huh, C. S., Ra, J., Choi, I. D., Jeong, J. W., Kim, S. H., et al. (2015). Clinical Evidence of Effects of *Lactobacillus Plantarum* HY7714 on Skin Aging: A Randomized, Double Blind, Placebo-Controlled Study. *J. Microbiol. Biotechnol.* 25(12), 2160–2168. doi: 10.4014/jmb.1509.09021
- Li, Z. C., Bai, X. Z., Peng, T. W., Yi, X. W., Luo, L., Yang, J. Z., et al. (2020). New Insights Into the Skin Microbial Communities and Skin Aging. *Front. Microbiol.* 565549. doi: 10.3389/fmicb.2020.565549
- Lim, H. Y., Jeong, D., Park, S. H., Shin, K. K., Hong, Y. H., Kim, E., et al. (2020). Antiwrinkle and Antimelanogenesis Effects of Tyndallized *Lactobacillus Acidophilus* KCCM12625P. *Int. J. Mol. Sci.* 21(5), 1620. doi: 10.3390/ijms21051620
- Lin, P. W., Myers, L. E., Ray, L., Song, S. C., Nasr, T. R., Berardinelli, A. J., et al. (2009). *Lactobacillus Rhamnosus* Blocks Inflammatory Signaling *In Vivo* via Reactive Oxygen Species Generation. *Free Radic. Biol. Med.* 124(1), 1205–1211. doi: 10.1016/j.freeradbiomed.2009.07.033
- Liu, J., Luo, J. G., Ye, H., Sun, Y., Lu, Z. X., and Zeng, X. X. (2009). Production, Characterization and Antioxidant Activities *In Vitro* of Exopolysaccharides From Endophytic Bacterium *Paenibacillus Polymyxa* EJS-3. *Carbohydr. Polym.* 78(2), 275–281. doi: 10.1016/j.carbpol.2009.03.046
- Liu, T., Song, X., An, Y., Wu, X., Zhang, W., Li, J., et al. (2021). *Lactobacillus Rhamnosus* GG Colonization in Early Life Ameliorates Inflammation of Offspring by Activating SIRT1/AMPK/PGC-1 α Pathway. *Oxid. Med. Cell. Longev.* 2021, 3328505. doi: 10.1155/2021/3328505
- Lloyd-Price, J., Arze, C., Ananthakrishnan, A. N., Schirmer, M., Avila-Pacheco, J., Poon, T. W., et al. (2019). Multi-Omics of the Gut Microbial Ecosystem in Inflammatory Bowel Diseases. *Nature* 69(7758), 655–662. doi: 10.1038/s41586-019-1237-9
- Luna, P. C. (2020). Skin Microbiome as Years Go by. *Am. J. Clin. Dermatol.* 21(Suppl 1), 12–17. doi: 10.1007/s40257-020-00549-5
- Mai, C., Qiu, L., Zeng, Y., and Tan, X. (2021). *Lactobacillus Casei* Strain Shirota Enhances the Ability of Geniposide to Activate SIRT1 and Decrease Inflammation and Oxidative Stress in Septic Mice. *Front. Physiol.* 12, 678838. doi: 10.3389/fphys.2021.678838
- Makrantonaki, E., Eckardt, R., Steinhagen-Thiessen, E., Gschnell, M., and Zouboulis, C. C. (2013). Skin Aging. *MMW Fortschr. Med.* 155Spec No 2, 50–55. doi: 10.1007/s15006-013-2130-3
- Mantzourani, I., Kazakos, S., Terpou, A., Alexopoulos, A., Bezirtzoglou, E., Bekatorou, A., et al. (2018). Potential of the Probiotic *Lactobacillus Plantarum* ATCC 14917 Strain to Produce Functional Fermented Pomegranate Juice. *Foods* 8(1), 4. doi: 10.3390/foods8010004
- Morita, A. (2007). Tobacco Smoke Causes Premature Skin Aging. *J. Dermatol. Sci.* 48(3), 169–175. doi: 10.1016/j.jdermsci.2007.06.015
- Naidoo, K., Hanna, R., and Birch-Machin, M. A. (2018). What is the Role of Mitochondrial Dysfunction in Skin Photoaging? *Exp. Dermatol.* 27(2), 124–128. doi: 10.1111/exd.13476

- Nurk, S., Bankevich, A., Antipov, D., Gurevich, A. A., Korobeynikov, A., Lapidus, A., et al. (2013). Assembling Single-Cell Genomes and Mini-Metagenomes From Chimeric MDA Products. *J. Comput. Biol.* 20(10), 714–737. doi: 10.1089/cmb.2013.0084
- Owens, K., Park, J. H., Schuh, R., and Kristian, T. (2013). Mitochondrial Dysfunction and NAD(+) Metabolism Alterations in the Pathophysiology of Acute Brain Injury. *Transl. Stroke Res.* 4(6), 618–634. doi: 10.1007/s12975-013-0278-x
- Page, A. J., Cummins, C. A., Hunt, M., Wong, V. K., Reuter, S., Holden, M. T., et al. (2015). Roary: Rapid Large-Scale Prokaryote Pan Genome Analysis. *Bioinformatics* 31(22), 3691–3693. doi: 10.1093/bioinformatics/btv421
- Park, J., Halliday, G. M., Surjana, D., and Damian, D. L. (2010). Nicotinamide Prevents Ultraviolet Radiation-Induced Cellular Energy Loss. *Photochem. Photobiol.* 86(4), 942–948. doi: 10.1111/j.1751-1097.2010.00746.x
- Patra, V., Gallais S  r  zal, I., and Wolf, P. (2020). Potential of Skin Microbiome, Pro- and/or Pre-Biotics to Affect Local Cutaneous Responses to UV Exposure. *Nutrients* 12(6), 1765. doi: 10.3390/nu12061795
- Poddar, S. K., Sifat, A. E., Haque, S., Nahid, N. A., Chowdhury, S., and Mehedi, I. (2019). Nicotinamide Mononucleotide: Exploration of Diverse Therapeutic Applications of a Potential Molecule. *Biomolecules* 9(1), 34. doi: 10.3390/biom9010034
- Scharffetter-Kochanek, K., Brenneisen, P., Wenk, J., Herrmann, G., Ma, W., Kuhr, L., et al. (2000). Photoaging of the Skin From Phenotype to Mechanisms. *Exp. Gerontol.* 35(3), 307–316. doi: 10.1016/s0531-5565(00)00098-x
- Scharschmidt, T. C., and Fischbach, M. A. (2013). What Lives on Our Skin: Ecology, Genomics and Therapeutic Opportunities of the Skin Microbiome. *Drug Discovery Today Dis. Mech* 10(3-4), e83-9. doi: 10.1016/j.ddmec.2012.12.003
- Thompson, B. C., Halliday, G. M., and Damian, D. L. (2015). Nicotinamide Enhances Repair of Arsenic and Ultraviolet Radiation-Induced DNA Damage in HaCaT Keratinocytes and Ex Vivo Human Skin. *PLoS One* 10, e0117491. doi: 10.1371/journal.pone.0117491
- Treangen, T. J., Ondov, B. D., Koren, S., and Phillippy, A. M. (2014). The Harvest Suite for Rapid Core-Genome Alignment and Visualization of Thousands of Intraspecific Microbial Genomes. *Genome Biol.* 15(11), 524. doi: 10.1186/s13059-014-0524-x
- Varani, J., Schuger, L., Dame, M. K., Leonard, C., Fligiel, S. E. G., Kang, S., et al. (2004). Reduced Fibroblast Interaction With Intact Collagen as a Mechanism for Depressed Collagen Synthesis in Photodamaged Skin. *J. Invest. Dermatol.* 122(6), 1471–1479. doi: 10.1111/j.0022-202X.2004.22614.x
- Vicentini, F. T., He, T., Shao, Y., Fonseca, M. J., Verri, W. A. Jr., Fisher, G. J., et al. (2011). Quercetin Inhibits UV Irradiation-Induced Inflammatory Cytokine Production in Primary Human Keratinocytes by Suppressing NF-  b Pathway. *J. Dermatol. Sci.* 61(3), 162–168. doi: 10.1016/j.jdermsci.2011.01.002
- Watson, R. E., Gibbs, N. K., Griffiths, C. E., and Sherratt, M. J. (2014). Damage to Skin Extracellular Matrix Induced by UV Exposure. *Antioxid. Redox Signal.* 21(7), 1063–1077. doi: 10.1089/ars.2013.5653
- Wu, L. E., and Sinclair, D. A. (2019). The Elusive NMN Transporter is Found. *Nat. Metab.* 1(1), 8–9. doi: 10.1038/s42255-018-0015-6
- Xu, C., Qiao, L., Guo, Y., Ma, L., and Cheng, Y. (2018). Preparation, Characteristics and Antioxidant Activity of Polysaccharides and Proteins-Capped Selenium Nanoparticles Synthesized by *Lactobacillus Casei* ATCC 393. *Carbohydr. Polym.* 195, 576–585. doi: 10.1016/j.carbpol.2018.04.110
- Yachida, S., Mizutani, S., Shiroma, H., Shiba, S., Nakajima, T., Sakamoto, T., et al. (2019). Metagenomic and Metabolomic Analyses Reveal Distinct Stage-Specific Phenotypes of the Gut Microbiota in Colorectal Cancer. *Nat. Med.* 25(6), 968–976. doi: 10.1038/s41591-019-0458-7
- Yau, Y. F., El-Nezami, H., Galano, J. M., Kundi, Z. M., Durand, T., and Lee, J. C. Y. (2020). *Lactobacillus rhamnosus* GG and Oat Beta-Glucan Regulated Fatty Acid Profiles Along the Gut-Liver-Brain Axis of Mice Fed With High Fat Diet and Demonstrated Antioxidant and Anti-Inflammatory Potentials. *Mol. Nutr. Food Res.* doi: 10.1002/mnfr.202000566
- Yiasemides, E., Sivapirabu, G., Halliday, G. M., Park, J., and Damian, D. L. (2009). Oral Nicotinamide Protects Against Ultraviolet Radiation-Induced Immunosuppression in Humans. *Carcinogenesis* 30(1), 101–105. doi: 10.1093/carcin/bgn248
- Ying, S., Zeng, D. N., Chi, L., Tan, Y., Galzote, C., Cardona, C., et al. (2015). The Influence of Age and Gender on Skin-Associated Microbial Communities in Urban and Rural Human Populations. *PLoS One* 12(8), e0141842. doi: 10.1371/journal.pone.0141842
- Zahran, W. E., Elsonbaty, S. M., and Moawed, F. S. M. (2017). *Lactobacillus Rhamnosus* ATCC 7469 Exopolysaccharides Synergizes With Low Level Ionizing Radiation to Modulate Signaling Molecular Targets in Colorectal Carcinogenesis in Rats. *Biomed. Pharmacother.* 92, 384–393. doi: 10.1016/j.biopha.2017.05.089
- Zeng, Y., Li, Y., Wu, Q. P., Zhang, J. M., Xie, X. Q., Ding, Y., et al. (2020). Artn 8818989. Evaluation of the Antibacterial Activity and Probiotic Potential of *Lactobacillus Plantarum* Isolated From Chinese Homemade Pickles. *Can. J. Infect. Dis. Med. Microbiol.* 2020, 1–11. doi: 10.1155/2020/8818989

Conflict of Interest: The authors declare that the research was conducted in the absence of any commercial or financial relationships that could be construed as a potential conflict of interest.

Publisher’s Note: All claims expressed in this article are solely those of the authors and do not necessarily represent those of their affiliated organizations, or those of the publisher, the editors and the reviewers. Any product that may be evaluated in this article, or claim that may be made by its manufacturer, is not guaranteed or endorsed by the publisher.

Copyright    2022 Chen, Li, Xie, Chen, Xue, Wang, Ye, Wu, Yang, Zhao, Zhang, Ding and Wu. This is an open-access article distributed under the terms of the Creative Commons Attribution License (CC BY). The use, distribution or reproduction in other forums is permitted, provided the original author(s) and the copyright owner(s) are credited and that the original publication in this journal is cited, in accordance with accepted academic practice. No use, distribution or reproduction is permitted which does not comply with these terms.